Journal of Catalysis **204,** 498–511 (2001)
doi:10.1006/jcat.2001.3398, available online at http://www.idealibrary.com on IDEAL®

Reforming of Methane with Carbon Dioxide over $Pt/ZrO_2/Al_2O_3$ Catalysts

Mariana M. V. M. Souza,* Donato A. G. Aranda,*,† and Martin Schmal*,†,[1]

*NUCAT/PEQ/COPPE, Universidade Federal do Rio de Janeiro, C.P. 68502, 21945-970, Rio de Janeiro, Brazil; and †Escola de Química, Universidade Federal do Rio de Janeiro, C.P. 68542, 21940-900, Rio de Janeiro, Brazil

Received July 5, 2001; revised August 31, 2001; accepted August 31, 2001

The kinetics of CO_2 reforming of methane was studied over Pt supported on Al_2O_3, ZrO_2, and x% ZrO_2/Al_2O_3 ($1 \leq x \leq 20$ wt%), and the catalysts were characterized using different techniques. The influence of the support on the catalyst activity and carbon deposition resistivity was markedly different in each case. Although the Pt/Al_2O_3 catalyst deactivated significantly within 20 h onstream at 1073 K, zirconia-containing catalysts exhibited much higher stability even after 60 h onstream. Thermogravimetric analysis results showed that the amount of carbon on Pt/Al_2O_3 is much larger than on Pt/ZrO_2. Temperature-programmed reduction, CO chemisorption, and Fourier transform infrared of CO results provided evidence of metal–support interactions on zirconia-containing catalysts, indicating that the suppression of carbon deposition over these systems is probably due to $Pt–Zr^{n+}$ interactions. A reaction mechanism was proposed involving two different pathways: CH_4 decomposition on metal particles and CO_2 activation on the support. A kinetic model based on this dual mechanism successfully correlated the experimental data.

Key Words: **reforming; methane; zirconia–alumina; platinum.**

INTRODUCTION

Methane reforming using carbon dioxide (dry reforming) has been of interest for a long time (1, 2), but in recent years it has grown for both environmental and commercial reasons. This process offers important advantages compared to steam reforming of methane. Namely, (a) it yields lower H_2/CO product ratios, which are preferable feeds for Fischer–Tropsch plants (3) and for synthesis of oxoalcohols (4) and acetic acid and dimethyl ether (5); (b) it reduces CO_2 and CH_4 emissions, which are both greenhouse gases; and (c) it is well suited for chemical energy transmission systems (6, 7).

The major disadvantage of CH_4–CO_2 reforming is the high thermodynamic potential in coke formation (3, 8). Much effort has been directed toward development of catalysts capable of operating under severe deactivation conditions. There are two commercial processes that have overcome the coking problem. The SPARG process (9) ameliorates the coke formation by using sulfur passivation of a Ni catalyst, which allows control of the ensemble size on the metal surface. The CALCOR process (10, 11) operates with special catalyst packing that prevents carbon deposition, but it is not described in detail. These processes have some drawbacks, such as the presence of sulfur compounds in the products. Thus, there are strong incentives to analyze the mechanistic aspects of dry reforming in order to produce stable catalysts.

Although development of catalysts based on nonnoble metals (e.g., Fe, Co, Ni) is of interest from the industrial point of view, numerous studies have demonstrated that noble metal catalysts exhibit better activity and suffer less carbon deposition (12–14). There is evidence that the support utilized can have a significant effect on the overall catalytic behavior (15, 16). Among zirconia-supported group VIII metals, Pt is one of the most active and stable metals (17). Van Keulen *et al*. (17) showed that Pt/ZrO_2 has great stability for a period over 1000 h, at 923–973 K and a feed ratio of $CH_4–CO_2 = 2$.

Bradford and Vannice (18) proposed that the higher stability and coking resistivity of Pt/ZrO_2 may be associated with strong $Pt–Zr^{n+}$ interactions, resulting in the formation of ZrO_x species on the Pt surface. Moreover, ZrO_2 seems to have a significant influence on the reaction mechanism of CH_4–CO_2 reforming, as shown recently (19–22). The mechanism involves two independent reaction paths: CH_4 decomposition on the metal particle and CO_2 activation on the support. Thus, the reaction takes place basically at the metal–support interface.

Despite the fact that CH_4–CO_2 reforming has been studied extensively, less emphasis has been given to fundamental understanding of the reaction kinetics. Bradford and Vannice proposed a complete and consistent reaction model for CH_4–CO_2 reforming, based on CH_4 activation to form CH_x and CH_xO decomposition as the rate-determining steps, fitting well the experimental data for Ni (23) and Pt catalysts (18). Although Bradford and Vannice (18, 23, 24) had considered the roles of three types of sites (metal, support, and metal–support interface), their proposed kinetic model only included one type of active site.

[1] To whom correspondence should be addressed. Fax: (5521) 2562-8300. E-mail: schmal@peq.coppe.ufrj.br.

0021-9517/01 $35.00

To our knowledge, the use of alumina-supported zirconia as a support for Pt in a CH_4–CO_2 reforming reaction has not been reported in the open literature. Dispersed zirconium oxide on alumina constitutes of a new class of attractive carriers because it combines the unique chemical properties of ZrO_2 with the high surface area and mechanical stability of alumina. Thus, the aim of this paper is to study the surface properties of $Pt/ZrO_2/Al_2O_3$ systems in order to investigate the role of the support in the catalytic behavior and to examine the coking resistance of supported Pt catalysts. The reaction mechanism of CH_4 reforming by CO_2 is discussed based on a kinetic model involving two reaction paths, which is correlated to the experimental data.

EXPERIMENTAL

Catalyst Preparation

Commercial γ-Al_2O_3 (Harshaw, Al3996) and ZrO_2, obtained by calcination of zirconium hydroxide (MEL Chemicals) in air at 823 K for 2 h, were used as supports.

ZrO_2/Al_2O_3 samples were prepared by impregnation over alumina powder with a nitric acid solution (50 vol%) of zirconium hydroxide. The mixture was stirred for 2 h at 363 K. The resulting solid was dried at 393 K for 16 h and calcined at 823 K for 2 h under flowing air. The estimated zirconia loadings were 1, 5, 10, and 20% (wt/wt). Zirconia contents were determined by X-ray fluorescence.

The Pt catalysts were prepared using the incipient wetness technique, using an aqueous solution of $H_2PtCl_6 \cdot 6H_2O$ (Aldrich), followed by drying at 393 K for 16 h and calcination in air at 823 K for 2 h. For all catalysts, the platinum content was around 1 wt%, which was determined by atomic absorption spectrometry. The prepared catalysts are referred to as PtAl for Pt/Al_2O_3, PtZr for Pt/ZrO_2, and Pt*x*Zr for Pt/*x* % ZrO_2/Al_2O_3.

Characterization

Textural properties were obtained in an ASAP 2000 apparatus (Micromeritics) after pretreatment under vacuum at 573 K. BET surface areas were determined from nitrogen isotherms at 77 K.

Temperature-programmed reduction (TPR) apparatus and methodology were described elsewhere (25). The samples were dehydrated at 423 K under flowing Ar before the reduction. A mixture of 1.65% hydrogen in argon flowed at 30 ml/min through the sample, raising the temperature at a heating rate of 10 K/min up to 973 K.

H_2 and CO chemisorption analyses were obtained at room temperature using an automatic adsorption system (ASAP 2000, Micromeritics). The samples were pretreated with He flux at 423 K for 1 h. After reduction at 573 or 773 K under 10% H_2/Ar flow, the samples were evacuated at 10^{-6} Torr for 30 min at the reduction temperature and cooled to room temperature. Irreversible H_2 and CO uptakes were obtained from the total and reversible adsorptions isotherms taken in a pressure range of 50–350 mm Hg.

Samples for infrared (IR) spectroscopy were in the form of self-supporting disks and weighed around 25 mg. The sample analysis was carried out with a Perkin-Elmer model 2000 Fourier transform infrared (FTIR) at a resolution of 2 cm^{-1}. The catalysts were dried at 423 K under vacuum, followed by reduction at 573 or 773 K with 10% H_2/Ar flux for 1 h and evacuation for 30 min. After cooling to room temperature, CO or CO_2 was admitted at 30 Torr for 15 min and after evacuation the IR spectrum was taken. This procedure was repeated for desorption temperatures at 323, 373, 473, and 573 K. All spectra were taken after cooling to room temperature. The absorbance spectra were obtained by using the interferograms of reduced samples as background references. The CO coverages at higher temperatures were obtained by dividing the total integrated area of linearly bonded CO vibration bands at each temperature by the total integrated area obtained after desorption at room temperature. The statistical variation relating to the number of measurements at various coverages was 3 cm^{-1}.

Catalyst Testing

Typically 20 mg of catalyst was loaded into a tubular quartz reactor and the catalyst bed temperature was measured by a thermocouple. The catalysts were dried *in situ* with flowing nitrogen at 423 K before reduction with 10% H_2/N_2 for 1 h at 773 K. After reduction the catalyst was purged with nitrogen for 30 min at the same temperature. All activity tests were carried out under atmospheric pressure with a feed composition of $CO_2/CH_4/He = 1/1/18$ and a total feed flow rate of 200 cm^3/min (weight-hourly space velocity = 600,000 $cm^3/h \cdot g\,cat$), over the temperature range 723–1173 K. The partial-pressure dependencies were determined by keeping 19 Torr of one reactant and varying the other reactant pressure between 7 and 57 Torr, while the balance of He was adjusted to maintain a total gas flow rate of 200 sccm. The reaction products were analyzed using an online gas chromatograph (CHROMPACK CP9001), equipped with a Hayesep D column and a thermal conductivity detector.

Spent catalysts were examined by thermal desorption analysis (TDA) and thermogravimetric analysis (TGA), using a RIGAKU thermoanalyzer (model TAS 100) operated in a 15% O_2/N_2 flow to check whether or not coke had been formed on the used catalyst.

RESULTS

Concentration and Surface Area

Platinum and zirconia loadings and BET surface areas for all catalysts are presented in Table 1. The 1–10% zirconia-containing samples showed specific area values close to that

TABLE 1

Chemical Composition and Surface Area

Catalyst	Pt (wt%)	ZrO_2 (wt%)	BET area (m^2/g)
PtAl	0.86	—	199
PtZr	0.83	—	62
Pt1Zr	0.80	0.64	183
Pt5Zr	0.87	4.00	190
Pt10Zr	0.95	8.28	180
Pt20Zr	0.85	19.10	147

TABLE 2

Temperature-Programmed Reduction Results

Catalyst	Experimental uptakes (μmol H_2/g cat)	Theoretical uptakes (μmol H_2/g cat)
PtAl	81.6	88.2
PtZr	129.1[a]	85.1
Pt1Zr	109.4	82.0
Pt5Zr	105.5	89.2
Pt10Zr	109.4	97.4
Pt20Zr	101.9[a]	87.2

[a] Calculated using integration of the first reduction peak only.

of alumina, while the loss in BET surface area was approximately 26% for the sample with 20% ZrO_2. Although the mean crystallite size of ZrO_2 in the Pt20Zr sample is only 1 nm, as measured by X-ray diffraction (26), alumina pores can be blocked by zirconia particles, decreasing the specific area of this sample. According to Damyanova *et al.* (27), a monolayer of zirconia is reached at a loading of 17 wt%. Our X-ray photoelectron spectroscopy and ion-scattering spectroscopy measurements (26) also proved that the surface coverage of zirconia on alumina increased up to 10%, and above this concentration, crystallites of ZrO_2 nucleated. Below the loading of 10 wt% the zirconia could be highly dispersed on alumina, even though the possibility of small ZrO_x islands or crystallites cannot be excluded.

TPR

The TPR profiles of the catalysts are displayed in Fig. 1. The experimental and theoretical H_2 uptakes are presented in Table 2, assuming the reduction $Pt^{4+} \rightarrow Pt^0$. Several authors in the literature support the evidence that Pt oxide is in the 4+ oxidation state in the dispersed phase of platinum catalysts (28, 29). The reduction profile of PtAl was similar to those reported in the literature (28, 30). The PtAl catalyst exhibited a maximum reduction rate at 553 K, which has been related to the reduction of an oxychloroplatinum surface complex, such as $[Pt(OH)_xCl_y]_s$ and $[PtO_xCl_y]_s$ (29). These results can be explained based on the specific capacity of alumina to retain chlorine ions.

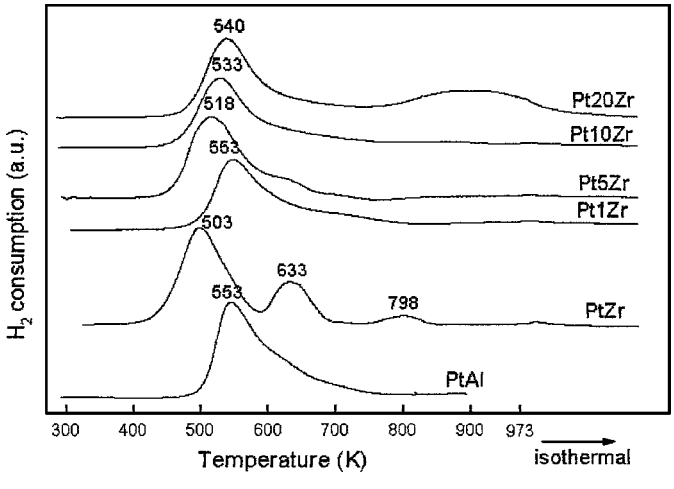

FIG. 1. TPR profiles for platinum catalysts. Conditions: 1.65% H_2/Ar, 10 K/min, and GHSV = 2118 $cm^3/h \cdot g$ cat.

The PtZr catalyst exhibited three main peaks, at 503, 633, and 798 K. The H_2 uptake corresponding to the first peak (503 K) was higher than that needed for complete platinum reduction (Table 2). As pure zirconia did not present H_2 consumption during TPR, the additional H_2 consumption by the PtZr catalyst may be associated to the reduction of zirconia at the metal interface. The easier reduction of platinum in this case, as seen by the TPR peak shift to lower temperatures, suggests the formation of chloride-free surface platinum oxides (α-PtO_2), because zirconia probably retains less chlorine. The other two peaks are attributed to the additional reduction of the support.

The alumina-supported zirconia catalysts also exhibited a small shift of the maximum peak to lower temperatures compared to that of the PtAl catalyst (with the exception of Pt1Zr), which can be explained by a lower amount of chlorine retained on that support, since an increased amount of zirconia covers the alumina surface. These catalysts displayed a shoulder around 623–673 K that shows the contribution of the support to the H_2 uptake presented in Table 2. The shoulder on Pt*x*Zr catalysts can be associated with the hydrogen spillover: the platinum, once reduced, can dissociate H_2 homolitically, with the formation of active species moving toward the zirconia surface, which helps the reduction of ZrO_2. Similar results were obtained by Yao and co-workers (31, 32) for metallic catalysts supported on CeO_2/Al_2O_3 and MoO_3/Al_2O_3.

The TPR profile of the Pt20Zr catalyst presented a second reduction peak at 893 K, which can be associated with the reduction of zirconia crystallites. A small peak was also observed at this temperature in the reduction profile of the 20% ZrO_2/Al_2O_3 support (not shown). For lower contents of zirconia there was no H_2 uptake in the metal absence until 973 K.

H_2 and CO Chemisorption

The amounts of irreversibly adsorbed H_2 and CO at room temperature are shown in Table 3. The dispersion was calculated assuming a Pt : H ratio of 1 : 1.

TABLE 3

H_2 and CO Chemisorptions on Pt Catalysts

Catalyst	Reduction at 573 K				Reduction at 773 K			
	H_2 uptake (μmol/g cat)	H/Pt	CO uptake (μmol/g cat)	CO/H_2	H_2 uptake (μmol/g cat)	H/Pt	CO uptake (μmol/g cat)	CO/H_2
PtAl	19.0	0.74	27.3	1.44	22.3	0.87	35.7	1.60
PtZr	14.6	0.57	57.1	3.92	8.8	0.34	60.9	6.92
Pt1Zr	16.7	0.65	31.7	1.89	24.9	0.97	47.8	1.92
Pt5Zr	18.2	0.71	41.5	2.28	21.5	0.84	49.9	2.32
Pt10Zr	18.4	0.72	44.7	2.42	21.1	0.82	57.3	2.72
Pt20Zr	15.9	0.62	27.2	1.71	15.3	0.60	46.0	3.01

After reduction at 773 K, the PtAl catalyst presented high H/Pt values, as well did the catalysts with zirconia content between 1 and 10%. The presence of oxychlorinated platinum complexes (PtO_xCl_y), observed using TPR, is responsible for the high dispersion of platinum on alumina (30) and even for Pt*x*Zr catalysts with low zirconia loading. According to Baker *et al.* (33) the high dispersion of platinum on alumina-supported titania catalysts indicates that an amorphous phase of titania covers alumina. Similarly, the high dispersion observed for the catalysts containing 1–10% ZrO_2 might also be associated with amorphous zirconia on alumina, as proposed by Damyanova *et al.* (27). However, after reduction at 573 K, the hydrogen and carbon monoxide uptakes on those catalysts decreased.

The Pt20Zr catalyst presented a low H/Pt ratio compared to the other supported oxide catalysts and this ratio remains constant for both reduction temperatures. Thus, the lower dispersion can be attributed to the lower specific surface area of the support and not to the decoration phenomena of the metallic particles by reduced support, as claimed for $Pt/Nb_2O_5/Al_2O_3$ catalysts (34). In this case, platinum may interact with both amorphous and crystalline zirconia phases.

The lower dispersion of the PtZr catalyst might be associated with the retention of small amounts of chlorine by zirconia, creating platinum oxide species instead of PtO_xCl_y, due to the lower specific surface area of zirconia as compared to alumina. On the other hand, zirconia might be partially reduced at the metal–support interface, resulting in ZrO_x moieties that migrate onto the platinum surface, decreasing the hydrogen uptake of the metal. When the PtZr catalyst is reduced at 573 K, the H_2 uptake was significantly higher, which suggests a smaller extent of zirconia reduction, as shown by TPR of PtZr.

The high values of the CO/H_2 ratio for zirconia-containing catalysts and, in particular, the PtZr catalyst reduced at 773 K predict that ZrO_2 modifies the Pt–CO and/or Pt–H bonds. Since the amount of adsorbed CO on pure zirconia is extremely low, the excess of CO is ascribed to the Pt–ZrO_x interface. The reversible CO adsorption was almost zero for all catalysts after reduction at 573 K, except for the PtZr catalyst. For this catalyst, the irreversible adsorption was constant for both reduction temperatures, while the reversible adsorption doubled at 773 K. This observation indicates that the irreversible adsorption might mainly characterize the metal, while the reversible part might be due to the metal–support interface, as proposed by Bonneviot and Haller (35). Indeed, the reversible uptake of CO on Pt/TiO_2 was attributed to the adsorption on Ti^{3+} ions and oxygen vacancies created in the vicinity of the Pt particles at high reduction temperatures:

$$Ti^{4+} - O - Ti^{4+} + H_2 \rightarrow Ti^{3+} - \bullet - Ti^{3+} + H_2O.$$

Vannice and Sudhakar (36) suggested that the adsorbed CO molecules interact via its oxygen atom with the oxygen-deficient TiO_x moieties residing around the Pt surface. The CO dissociation may be assisted by the reoxidation of the TiO_x moieties.

FTIR of CO and CO_2

Figure 2 presents the FTIR spectra of CO adsorbed on the PtAl, PtZr, Pt10Zr, and Pt20Zr catalysts after desorption at 298 (Fig. 2A) and 473 K (Fig. 2B). The peaks between 2070 and 2082 cm^{-1} are attributed to the linearly bonded CO on platinum at room temperature. Negligible amounts of bridge-bonded CO (1780–1860 cm^{-1}) were observed on alumina-supported catalysts. Noteworthy is the peak around 1540–1650 cm^{-1} on zirconia-containing catalysts, which can be attributed to carbonate species on the support (37, 38). A possible assignment of this peak to surface formate species was excluded because of the absence of C–H vibrations in the spectral region 2800–3000 cm^{-1}, according to He and Ekerdt (39, 40).

The spectra of CO adsorption on alumina-supported zirconia catalysts were very similar to the PtAl catalyst spectrum, not showing the role of the zirconia on CO adsorption, as observed by chemisorption measurements. On the other hand, the IR spectrum of the PtZr catalyst reduced at 773 K provided essential information about the nature of the metal–support interaction. A small band is presented at 2178 cm^{-1} at 298 K, attributed to the linear adsorbed

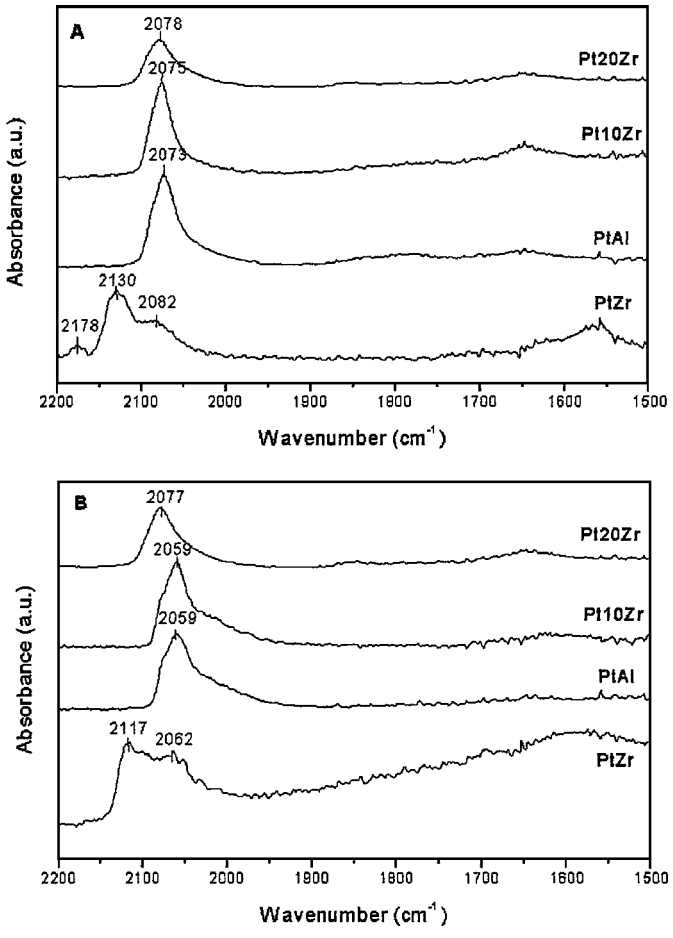

FIG. 2. Infrared spectra of CO for platinum catalysts reduced at 773 K with spectra obtained at the following desorption temperatures: (A) 298 K and (B) 473 K.

CO species on cationic sites (either Zr^{4+} or Zr^{3+}). This adsorption involves the σ-donation type to coordinatively unsatured surface cationic sites, acting as Lewis acid centers, according to previous works (41, 42).

The PtZr catalyst reduced at 773 K also showed an intense band at 2130 cm^{-1}, which is attributed to CO adsorbed on the Pt–ZrO_2 interface, that is, on Pt sites interacting strongly with zirconia. The increase in the vibration frequency of CO suggests an electron transfer phenomenon from platinum particles to partially reduced zirconia, which decreases the Pt–CO bond strength.

For PtZr catalyst reduced at 573 K the linearly adsorbed CO band was close to that observed for the PtAl catalyst, but with lower intensity and complete desorption at 573 K (not shown), indicating the weakness of the Pt–CO bond on a zirconia support.

CO peak maxima were plotted as a function of CO coverage (obtained by thermal desorption experiments) on platinum catalysts and the curves were extrapolated to zero surface coverage to determine the vibration frequency of isolated CO molecules. Table 4 shows the CO singleton vibration frequency for all catalysts. For all alumina-supported catalysts the extrapolation frequency of linearly adsorbed CO bands was observed around 2040–2047 cm^{-1}. For the PtZr catalyst there was a large increase in the frequency value assigned to $\lambda(\theta = 0)$, mainly after reduction at 773 K.

The vibration frequency of a single adsorbed CO molecule is related to the coordination number of the surface Pt atom to which CO is adsorbed: the lower the singleton frequency, the lower the coordination number (43). Thus, the increase in the singleton frequency of CO adsorbed on the PtZr catalyst indicates a higher coordination number of Pt atoms on the surface of this catalyst, which decreases the metal–CO back-bonds. Therefore, it justifies proposing an electron transfer phenomenon from Pt particles to partially reduced zirconia, decreasing the Pt–CO bond strength.

Figure 3 displays the thermal desorption FTIR spectra of CO_2 adsorbed on the PtZr catalyst reduced at 773 K (Fig. 3A) and bare ZrO_2 (Fig. 3B). The bands between 1550 and 1650 cm^{-1} are attributed to carbonate species on the support. The peaks at 1566 and 1326 cm^{-1} can be assigned to bidentate carbonate and the bands at 1618, 1439, and 1221 cm^{-1} stem from hydrogen carbonate species (37, 44). As for the thermal stability of different carbonate species we can observe that bidentate species still remain at the ZrO_2 surface upon evacuation at 573 K, while hydrogen carbonates are eliminated at ca. 373 K. Moreover, the stability of carbonates is greater on the bare support than on the PtZr catalyst.

At room temperature, CO_2 adsorbs as carbonate species on Zr^{n+} centers of the PtZr catalyst, and while temperature increases, these species are activated and migrate to metal particles, being desorbed as CO species. Thus, CO_2 activation on zirconia catalysts involves support and interfacial sites.

FTIR of CO_2 adsorbed on PtAl and Pt10Zr catalysts (Fig. 4) also showed the formation of carbonate species on the support and CO activation on the metal. However, CO desorption for the Pt10Zr catalyst with increased temperature is much slower than that for PtAl or PtZr catalysts, and CO remains on the surface up to 573 K.

TABLE 4

CO Singleton Vibration Frequency for Platinum Catalysts

Catalyst	Temperature reduction (K)	$\lambda\ (\theta = 0)\ cm^{-1}$
PtAl	773	2047
PtZr	573	2057
PtZr	773	2086
Pt1Zr	773	2041
Pt5Zr	773	2043
Pt10Zr	773	2043
Pt20Zr	773	2040

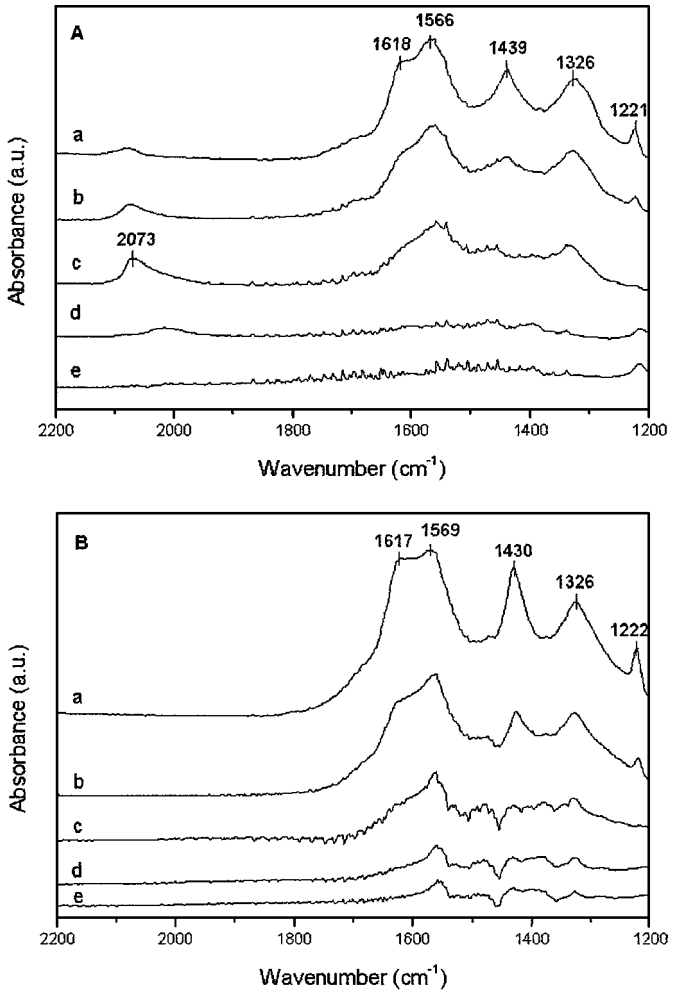

FIG. 3. Thermal desorption infrared spectra of CO_2 for a PtZr catalyst reduced at 773 K (A) and bare ZrO_2 (B), with spectra obtained at the following desorption temperatures: (a) 298 K, (b) 323 K, (c) 373 K, (d) 473 K, and (e) 573 K.

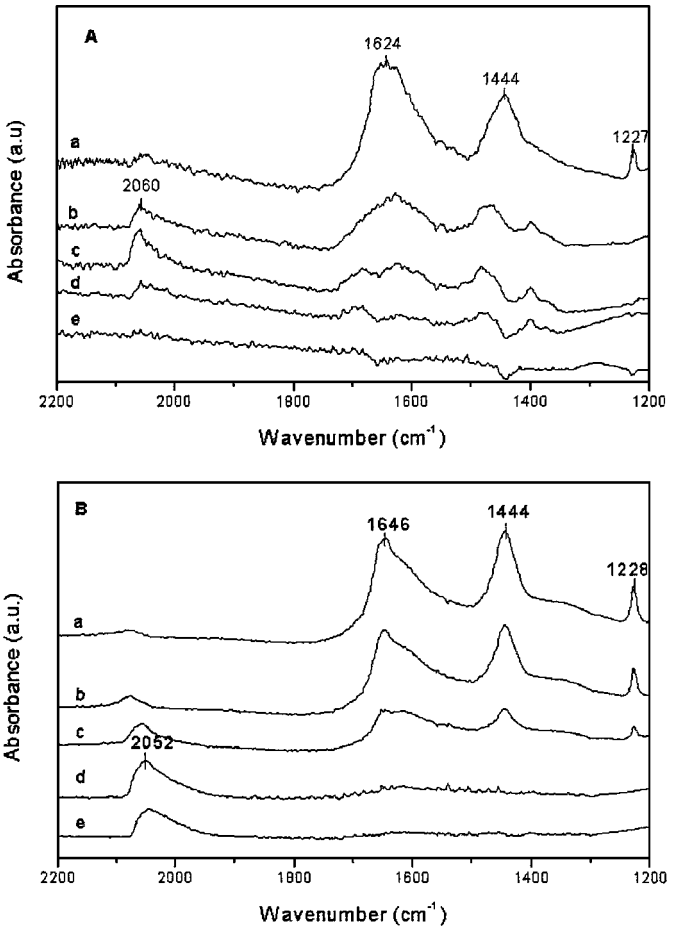

FIG. 4. Thermal desorption IR spectra of CO_2 for PtAl (A) and Pt10Zr catalysts (B) reduced at 773 K, with spectra obtained at the following desorption temperatures: (a) 298 K, (b) 323 K, (c) 373 K, (d) 473 K, and (e) 573 K.

Catalytic Tests

The effects of the temperature on the CH_4 conversions were measured under reforming conditions for all catalysts and the results are shown in Fig. 5. The catalytic performance of supported Pt catalysts for the reforming of methane with CO_2, in terms of initial activity, is strongly influenced by the support. At lower temperatures, PtZr was slightly less active, and at higher temperatures, PtAl and Pt1Zr were the least active. Pt10Zr was the most active catalyst over the whole temperature range investigated: the CH_4 conversion ranged from 5.5% at 723 K to 93.5% at 1173 K. The activity of the Pt5Zr and Pt20Zr catalysts, not shown in Fig. 5, was similar to the Pt10Zr at low temperatures but slightly lower at higher temperatures.

The methane conversion was always lower than the CO_2 conversion, although they were present in the feed in a 1 : 1 ratio, which is ascribed to the simultaneous occurrence of

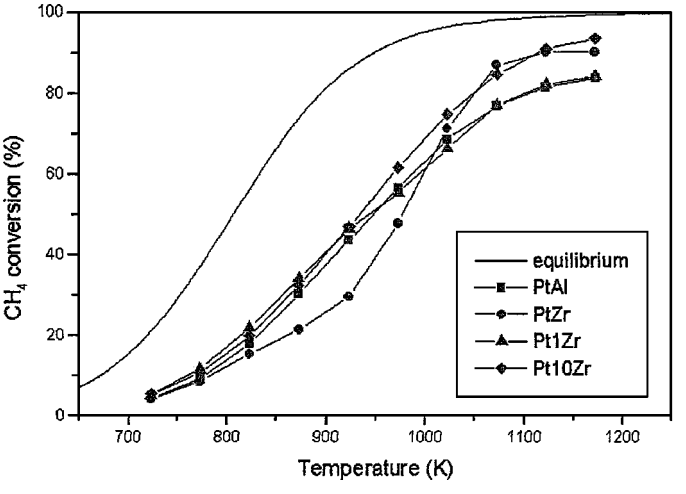

FIG. 5. CH_4 conversion of Pt catalysts during CO_2/CH_4 reforming as a function of temperature (each point was taken after 30 min onstream). Reaction conditions: $CH_4/CO_2/He = 1/1/18$; total feed flow rate = 200 cm^3/min.

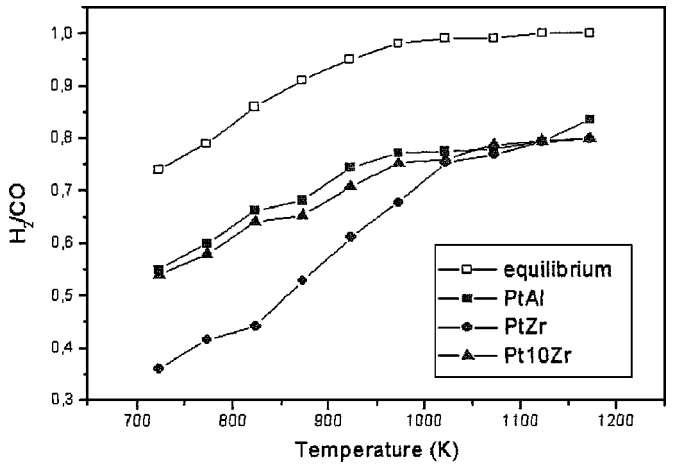

FIG. 6. H_2/CO product ratio of Pt catalysts during CO_2/CH_4 reforming as a function of temperature. Reaction conditions: $CH_4/CO_2/He = 1/1/18$; total feed flow rate = 200 cm^3/min.

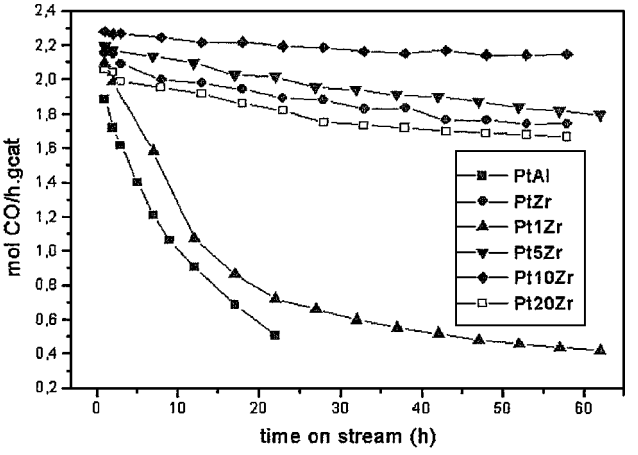

FIG. 8. The influence of aging at 1073 K on the CO production over the various Pt catalysts. Reaction conditions: $CH_4/CO_2/He = 1/1/18$; total feed flow rate = 200 cm^3/min.

the reverse water–gas shift reaction (RWGS):

$$CO_2 + H_2 \leftrightarrow CO + H_2O \quad \Delta H_{298K} = 41 \text{ KJ/mol.} \quad [1]$$

This also accounts for the observation that the H_2/CO ratio was always smaller than 1, tending to 1 at higher temperatures, as shown in Fig. 6. At low temperatures, the H_2/CO ratio was significantly lower for the PtZr catalyst, due to the small rate of H_2 formation over this catalyst, when compared to the others. Rostrup-Nielsen and Bak Hansen (14) have shown that the water–gas shift reaction is extremely rapid under typical methane reforming conditions. For this reason, RWGS is frequently assumed to be at equilibrium in the kinetic analysis during CH_4–CO_2 reforming (23, 45).

Stability tests were performed at 823 and 1073 K, and the results are shown in Figs. 7 and 8, respectively. The same order of activity maintenance was revealed at both temperatures: Pt10Zr > Pt5Zr ≥ Pt20Zr, PtZr ≫ Pt1Zr > PtAl. The PtAl and Pt1Zr catalysts exhibited high linear deactivation rates of $4.0 \pm 0.5\%$/h and $3.3 \pm 0.4\%$/h, respectively, during the first 20 h onstream at 1073 K, due to the fast deposition of inactive carbon, as discussed later. The Pt10Zr catalyst deactivated only at a rate of 0.1%/h during 60 h onstream at this same temperature. This catalyst displayed CH_4 and CO_2 conversions at 1073 K of 82 and 91%, respectively, which are close to thermodynamic equilibrium. Thus, the Pt10Zr catalyst exhibited excellent stability under conditions where carbon deposition is thermodynamically favorable (3).

The amount of carbon formation over PtAl and PtZr catalysts during the reaction at 1073 K was determined by TGA measurements, carried out in an oxygen-containing atmosphere (Fig. 9). The stable behavior of PtZr appears to be associated with the observation of little coke formation

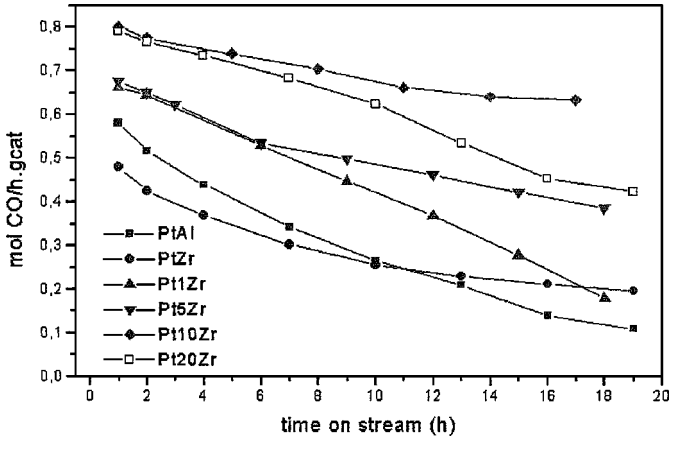

FIG. 7. The influence of aging at 823 K on the CO production over the various Pt catalysts. Reaction conditions: $CH_4/CO_2/He = 1/1/18$; total feed flow rate = 200 cm^3/min.

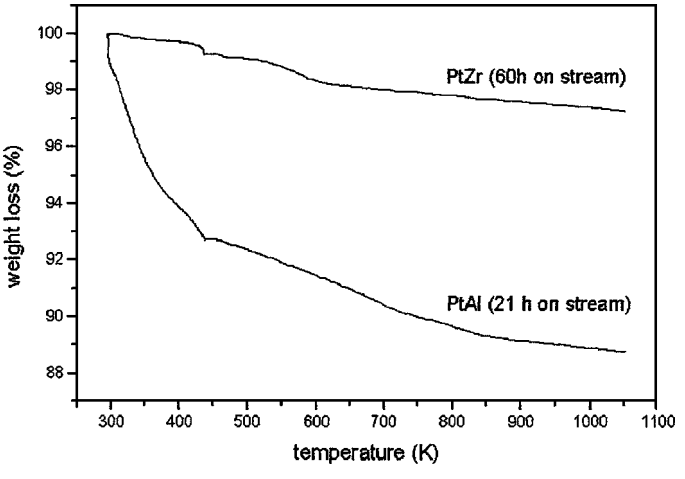

FIG. 9. TGA of PtAl and PtZr catalysts after reaction at 1073 K. Conditions: 15% O_2/N_2, 10 K/min; feed flow rate = 50 cm^3/min.

TABLE 5

Initial Catalyst Activity at 823 K and Apparent Activation Energies

Catalyst	Conversion (%)[a]		Activity[b]			E_{app} (Kcal/mol)[e]			
	CH_4	CO_2	mol CO/h · g cat	TOF_{CO}[c] (s^{-1})	TOF_{CH_4}[c] (s^{-1})	CH_4	CO_2	CO	H_2
PtAl	22.0	28.3	0.58	3.6	1.7	22.5	20.2	18.5	19.3
PtZr	13.9	21.5	0.48	2.2[d]	0.77[d]	18.4	15.0	15.0	12.8
Pt1Zr	23.5	30.9	0.66	3.7	1.6	15.5	14.6	14.6	15.2
Pt5Zr	22.7	31.3	0.68	4.4	1.8	13.1	16.4	15.1	17.1
Pt10Zr	26.6	36.2	0.80	5.3	2.2	14.8	14.1	14.4	17.3
Pt20Zr	28.9	36.8	0.79	4.8[d]	2.1[d]	16.2	15.2	14.1	16.0

[a] Equilibrium conversions of CH_4 and CO_2: 55.9 and 66.4%, respectively.
[b] Initial activity after 1 h onstream.
[c] Calculated from irreversible H_2 uptake after reduction at 773 K, except where noted.
[d] Calculated from irreversible CO uptake after reduction at 773 K.
[e] Calculated from Arrhenius plots with temperatures ranging between 733 and 823 K.

during the reaction. On the other hand, TGA experiments showed a weight loss of about 12% on treating the PtAl catalyst in oxygen, indicating a significant amount of carbon deposition over the course of 21 h onstream (5.7 mg coke/g cat · h).

The initial reaction rates at 823 K (mol/h · g cat) were normalized to the number of Pt surface atoms as measured by chemisorption of H_2 and CO (Table 3) to provide turnover frequencies (TOFs), as shown in Table 5. It is worth being cautious on analyzing the real morphology of the Pt surface under reaction conditions, due to the coverage of the Pt surface by ZrO_x species after reduction at 773 K. Thus, for PtZr and Pt20Zr catalysts, the initial TOF values for both CO production and CH_4 consumption were calculated from the irreversible CO uptake after reduction at 773 K, because H_2 uptake after reduction at this temperature is strongly influenced by the presence of ZrO_x species. The TOF values were not calculated using the results of chemisorption after reduction at 573 K because H_2 produced during reforming reaction at 823 K could induce the partial reduction of zirconia. The initial TOF values at 823 K increased with zirconia loading until 10 wt%, which is consistent with stability tests (Figs. 7 and 8). The conversions of CH_4 and CO_2 at 823 K ranged from one-fourth to half of the calculated equilibrium conversions of 55.9 and 66.4%, respectively.

Table 5 also presents the apparent activation energies for the consumption of CH_4 and CO_2 as well as for the production of CO and H_2. These energies were calculated from Arrhenius plots, such as those in Fig. 10, for CO production. The apparent activation energies were very similar for zirconia-contained catalysts and were lower than those for PtAl. It is noteworthy that the activation barrier for CH_4 consumption is higher than that for CO_2 consumption, in agreement with reported values in the literature (15). Also, the apparent activation energies for H_2 production are greater than those for the CO formation (except for the PtZr catalyst), which is probably ascribable to the occurrence of the RWGS.

The effect of partial pressures of CH_4 and CO_2 on the rate of CH_4 consumption was determined for PtAl, PtZr, Pt10Zr, and Pt20Zr catalysts, at 823 K, as shown in Fig. 11. When the partial pressure of CH_4 was held constant at 19 Torr, the rate of reaction of CH_4 exhibited two different levels, one when $P_{CO_2} < P_{CH_4}$ and other when $P_{CO_2} \geq P_{CH_4}$. When the CO_2 partial pressure was kept at 19 Torr, the rate of CH_4 consumption rose with the increase in CH_4 partial pressure up to 27 Torr; for higher pressures the rate was almost constant. The behavior of these catalysts is qualitatively similar, indicating the same reaction mechanism.

The influence of H_2 addition to the feed stream ($P_{CH_4} = P_{CO_2} = 30.4$ Torr) was also examined for PtAl, PtZr, and Pt10Zr catalysts at 823 K, as shown in Fig. 12. The effect of hydrogen in the feed is to increase CO_2 conversion

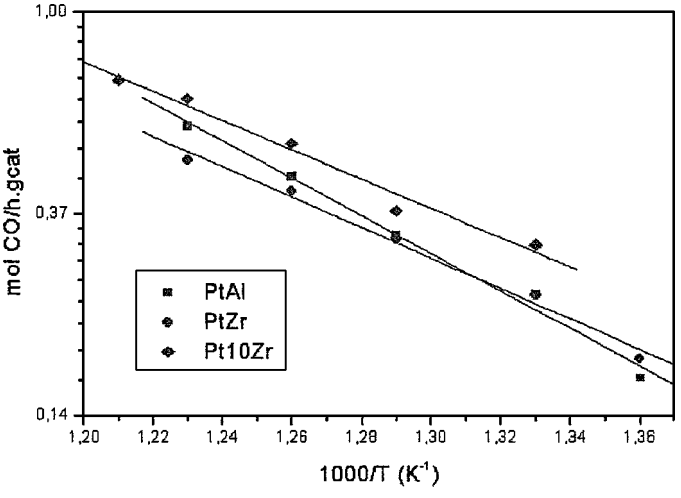

FIG. 10. Arrhenius plots for CO production (mol CO/h · g cat) over temperatures ranging between 733 and 823 K. Reaction conditions: $CH_4/CO_2/He = 1/1/18$; total feed flow rate = 200 cm^3/min.

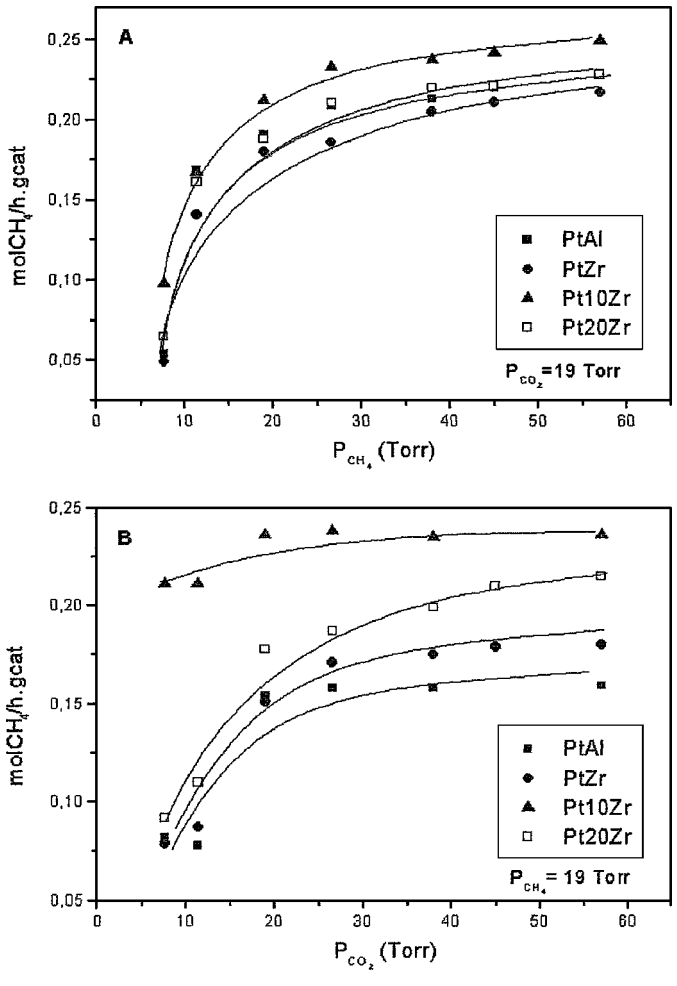

FIG. 11. Dependence of the rate of methane consumption on CH_4 partial pressure (A) and CO_2 partial pressure (B) at 823 K. Reaction conditions: atmospheric pressure and total feed flow rate = 200 cm^3/min.

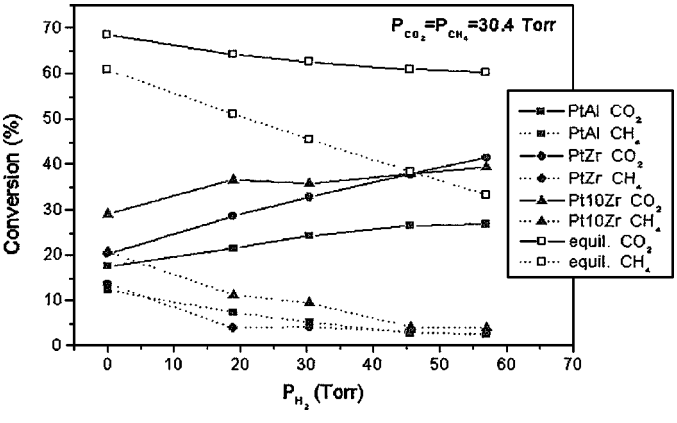

FIG. 12. Comparison of the observed influence of H_2 addition to the feed stream with that calculated from thermodynamic equilibrium for PtAl, PtZr, and Pt10Zr at 823 K. Reaction conditions: $CH_4/CO_2/H_2/He = 1/1/n/18\text{-}n$; total feed flow rate = 200 cm^3/min.

due to RWGS and to inhibit CH_4 consumption. Under the pressure range analyzed, thermodynamic calculations did not predict CH_4 formation, but it has been shown that at higher pressures methanation was also possible (18, 23).

DISCUSSION

The Role of the Support

The results presented in this contribution showed that the support plays a decisive role on the activity and stability of the catalyst. PtAl deactivated quickly during the first 20 h of CH_4–CO_2 reforming at 1073 K (Fig. 8), while zirconia based catalysts (with ZrO_2 content $\geq$5%) presented a very stable performance over the course of 60 h. There are three different possibilities that may explain this behavior: the dispersion of platinum or sintering, the interaction of Pt with Zr^{n+} centers on the support, and the surface acidity/basicity of the support.

Van Keulen and co-workers (17) have proposed that the stable behavior of the Pt/ZrO_2 catalyst is associated to the ability of zirconia to anchor the Pt particles, explaining it in terms of a formation of a Pt–Zr surface alloy that helps to maintain a high Pt dispersion at high reaction temperatures. However, extended X-ray absorption fine structure data presented by Stagg *et al.* (21) provided evidence that Pt is in an unmodified metallic state. Sintering of Pt particles can be discarded due to the high level of dispersion obtained by reducing the zirconia-containing samples at 573 and 773 K. Bitter *et al.* (46, 47) also excluded sintering during reforming conditions based on the results for Pt/Al_2O_3 and Pt/ZrO_2 catalysts.

Our TGA results showed that the amount of carbon formed over PtAl is much larger than that formed on the PtZr catalyst (Fig. 9). Seshan *et al.* (48) also used differential scattering calorimeter/TGA to show that the Pt/ZrO_2 catalyst exhibits little or no carbon formation during CH_4–CO_2 reforming after 500 h onstream at 853 K. The higher stability and coking resistivity of Pt/ZrO_2 may be related to strong Pt–Zr^{n+} interactions. Indeed, the TPR analyses indicated that zirconia can be reduced at temperatures lower than 500 K, resulting in ZrO_x species that may decorate the Pt surface, diminishing hydrogen chemisorption capacity (Table 3). This so-called strong metal–support interaction (SMSI) effect was already observed by Bitter *et al.* (19) for the Pt/ZrO_2 catalyst, but they stated that during the reaction, this SMSI state is absent since the dissociation of CO_2 produces adsorbed oxygen species that reoxidize the ZrO_x species. As H_2 is produced by the reforming reaction, it is unclear whether or not the SMSI effect occurs during reaction conditions. When zirconia is dispersed over alumina, ZrO_x species seem to have less mobility than on the PtZr catalyst, because there was no suppression of H_2 chemisorption after reduction at 773 K for PtxZr catalysts ($x \leq 10\%$). Besides,

there was a little increase in H_2 uptake after reduction at 773 K, compared to 573 K, which indicated that the Pt surface should not be extensively recovered by ZrO_x species.

Chemisorption results clearly showed that Pt–Zr^{n+} interactions modify the adsorption of CO on the Pt surface, increasing the reversible uptake of CO. Roberts and Gorte (49) have examined Pt overlayers on ZrO_2 (100) and showed that for submonolayer Pt coverage, interaction exists between Pt and Zr^{4+} cations at the surface, which significantly decreases the CO desorption temperature. Comparing temperature-programmed desorption and high-resolution electron energy loss spectroscopy results, Dilara and Vohs (50) correlated the downward shift in desorption temperature with the appearance of CO species bounded at the Pt–ZrO_2 interface. In the bonding configuration proposed, the carbon end of the CO molecule is bounded to the metal, while the oxygen end interacts with a zirconium cation on the surface of the oxide. This configuration may also explain the intense band at 2130 cm^{-1} observed in the FTIR spectra of CO adsorbed on the PtZr catalyst (Fig. 2A). Moreover, our IR results (Table 4) pointed to a decrease in the Pt–CO bond strength on the PtZr system, which indicates that zirconia inhibits the CO disproportionation on platinum surface. Thus, the intensity of back donation is lower in the CO/electron-deficient platinum model. The main consequence is a lower amount of carbon on the surface and even a larger stability during the reaction.

Inactive carbon during methane reforming can be originated not only from CO disproportionation, but also from methane decomposition:

$$CH_4 \leftrightarrow C + 2H_2 \quad \Delta H_{298K} = 75 \text{ KJ/mol}, \qquad [2]$$

$$2CO \leftrightarrow CO_2 + C \quad \Delta H_{298K} = -172 \text{ KJ/mol}. \qquad [3]$$

Thermodynamic calculations presented by Reitmeier *et al.* (51) and Gadalla and Bower (3) showed that for any reaction mixture of CH_4, CO_2, CO, H_2, and H_2O at thermodynamic equilibrium, the extent of carbon deposition during reforming decreases at higher reaction temperatures, in agreement with numerous experimental observations (6, 17, 23). These results suggest that CO disproportionation is the main contributor to carbon deposition, because it is exothermic and the equilibrium constant decreases with the increase in the temperature. In addition, Swaan *et al.* (45) and Efstathiou *et al.* (52) showed by TPO with isotopic mixtures that most of the carbon accumulated during the reforming reaction is derived from a CO_2 molecule, suggesting that CH_4 decomposition is not the principal carbon formation mechanism.

Carbon suppression on zirconia-containing catalysts may also be associated with the control of ensemble size on the metal surface. Some theoretical calculations showed that CO dissociation requires an ensemble size of four or five metal atoms (53); so the presence of ZrO_x species over the Pt surface reduces the number of large ensembles of Pt atoms, geometrically inhibiting CO dissociation. The ZrO_x decoration phenomena may also inhibit CH_4 decomposition. Minot *et al.* (54) studied the adsorption of CH_x species on Pt(111) using the extended Hückel theory. These investigations indicated that carbon is located on the surface in such a way as to complete its tetravalency. It implies that the stepwise decomposition of CH_4 on Pt requires concomitant occupation of higher coordination sites. Thus, the covering of the Pt surface by ZrO_x species can inhibit complete CH_4 decomposition.

It has been suggested that the carbon deposition is suppressed when the metal is supported on metal oxide with strong Lewis basicity (55, 56). Increasing Lewis basicity of the support increases the ability of catalysts to adsorb CO_2, which reduces the carbon deposition via CO disproportionation by shifting the equilibrium toward the left (Reaction [3]). The electron transfer phenomenon from Pt particles to partially reduced zirconia, as indicated by FTIR spectra of CO adsorbed on a PtZr catalyst, increases the basicity of the support. The enhancement of CO_2 adsorption in zirconia-containing catalysts was also shown by FTIR of CO_2 on Pt10Zr (Fig. 4). This is more evidence for the coking resistance of zirconia catalysts.

Bitter *et al.* (47) have shown that carbon is formed not only in metal-containing catalysts but also on pure supports. The presence of Lewis acid sites facilitates the cleavage of methane C–H bond (57); thus, these sites are active for carbon deposition. According to these authors, Pt seems to selectively block Lewis acid sites for Pt/ZrO_2, while for Pt/Al_2O_3 a significant fraction remains after Pt deposition, as also suggested by Masai *et al.* (58). However, our IR spectroscopy of adsorbed pyridine (59) revealed a higher concentration of Lewis acid sites on PtZr compared with PtAl. As the amount of carbon formation on zirconia-containing catalysts was lower than on PtAl, it seems that there is not a straight relation between the acidity of the support and the carbon deposition under reaction conditions.

The initial activities based on TOF values (Table 5) are similar for all catalysts; however, PtZr exhibited a somewhat lower value, based on CO adsorption after reduction at 773 K. Bradford and Vannice (18) reported that initial TOFs for CO production and CH_4 consumption at 723 K for 0.31% Pt/ZrO_2 were 1.1 and 0.39 s^{-1}, respectively, based on total H_2 uptake after reduction at 773 K (dispersion of 82%). Considering the differences in temperature and partial pressures to our work, these values can be recalculated to 3.0 and 1.3 s^{-1} [reaction orders were obtained in Ref. (15)], which are higher than those for PtZr. However, these values were lower than those for alumina-supported catalysts. The lower TOF values for the PtZr catalyst may be related to methane activation. C–H bond cleavage requires electron donation from the surface to any of the lowest

unoccupied antibonding molecular orbitals on methane. Since a Pt particle is electron deficient in a PtZr catalyst, its ability to activate C–H bond cleavage is lower, resulting in lower specific activities.

The activation energy obtained with PtZr for carbon monoxide formation, 15 Kcal/mol, is in good agreement with the values of 21.6 Kcal/mol, obtained by Bradford and Vannice (18) and 15 Kcal/mol, calculated from the data reported by Seshan *et al*. (48). The activation energies obtained on the PtAl catalyst are also in fair agreement with values reported in the literature. From the data of Solymosi *et al*. (60) it is possible to obtain a value of 15 Kcal/mol for CH_4 consumption and 12 Kcal/mol for CO_2, over 2% Pt/Al_2O_3. It is noteworthy that the apparent activation energies for PtAl are higher than those for zirconia containing catalysts (Table 5). This suggests that the ability of zirconia to adsorb CO_2 is more important than the activation of CH_4, because PtAl has greater capacity to break C–H bonds due to the higher electron density on platinum. Although few investigations have reported apparent activation energies for CH_4–CO_2 reforming over supported Pt, the available values are always higher for CH_4 consumption than for CO_2 consumption, in agreement with our results.

Reaction Mechanism and Kinetics

One of the first reports of the kinetics of CO_2 reforming of CH_4 was in 1967 by Bodrov and Apel'baum (61), using Ni foil as the catalytic material. They proposed that the CO_2 reforming reaction could be described by a similar rate expression to that for steam reforming, based on the assumption that CH_4 does not react directly with CO_2, but with H_2O from the RWGS. Since this first work, and especially in the past 5 or 6 years, several authors have proposed different reaction mechanisms for CH_4–CO_2 reforming (6, 12, 14, 20, 21), but only a few of them reported kinetic equations.

Richardson and Paripatyadar (6) provided an expression based on the Langmuir–Hinshelwood approach involving redox mechanisms, for a Rh/Al_2O_3 catalyst. Zhang and Verykios (56) also proposed this reaction model for Ni/Al_2O_3 but neither of them presented the mechanisms from which they derived their models. Mark *et al*. (62) showed that classical heterogeneous models, like Eley–Rideal and Langmuir–Hinshelwood mechanisms, are not suitable for describing the kinetics of a CH_4–CO_2 reforming reaction over the whole temperature range. They proposed a rate model based on the stepwise mechanism, where in the rate-determining step methane is decomposed to H_2 and active carbon, followed by direct and fast conversion of this carbon with CO_2 to CO. This model led to a good fit for the data obtained on an Ir/Al_2O_3 catalyst in the temperature range of 973–1123 K.

One of the most comprehensive studies of the kinetics of CO_2 reforming was performed by Bradford and Vannice, who gave a detailed reaction mechanism for Ni (23) and Pt catalysts (18). This mechanism is based on CH_4 activation, forming CH_x and CH_xO decomposition as the slow kinetics steps. Carbon dioxide takes part in the reaction mechanism only through the RWGS reaction to produce surface OH groups that react with the adsorbed CH_x intermediates to yield formate species (CH_xO). The authors assumed that nondissociative adsorption of CO_2 under reaction conditions occurred on the support, but they did not consider two different types of active sites in their reaction model (a metal site and a support site).

However, previous studies (21, 22, 63) have provided evidence that on a Pt/ZrO_2 catalyst, the decomposition of CH_4 and the dissociation of CO_2 occur via two independent paths. The first path involves the decomposition of CH_4 on a metal particle, resulting in the production of H_2 and atomic carbon that partially reduces the oxide support near the metal particle. In the second path, CO_2 adsorbs on ZrO_x, replenishing the oxygen vacancy in the support, and thus providing a constant source of oxygen in a redox mechanism. TAP experiments carried out by Van Keulen *et al*. (64) over Pt/ZrO_2 also pointed to the presence of an oxygen pool, with the CO_2 acting as the supplier of oxygen to this pool.

Therefore, after analyzing the data available in the literature and the results obtained, the following bifunctional mechanism (where **p** is a platinum site and **z** a support site) is proposed for CH_4–CO_2 reforming:

(a) $CH_4 + \mathbf{p} \overset{k_{CH_4}}{\underset{K_{CO_2}}{\rightleftharpoons}} CH_x\text{-}\mathbf{p} + (\frac{4-x}{2})H_2$,
(b) $CO_2 + \mathbf{z} \longleftrightarrow CO_2\text{-}\mathbf{z}$,
(c) $H_2 + 2\mathbf{p} \leftrightarrow 2H\text{-}\mathbf{p}$,
(d) $CO_2\text{-}\mathbf{z} + 2H\text{-}\mathbf{p} \leftrightarrow CO + H_2O$,
(e) $CO_2\text{-}\mathbf{z} + CH_x\text{-}\mathbf{p} \overset{k}{\rightarrow} 2CO + \frac{x}{2}H_2 + \mathbf{z} + \mathbf{p}$.

The reversible CH_4 dissociative adsorption [step (a)] was also proposed by Bradford and Vannice (18, 23) and is supported by the effect of H_2 addition to the feed stream (Fig. 12), which showed that the CH_4 consumption was not at thermodynamic equilibrium. The formation of CH_x fragments on transition metal surfaces has been detected using H_2–CD_4 exchange reaction on Ni/MgO (5), D_2–CH_4 exchange on Rh/MgO (8), and CO_2 reforming of CH_4/CD_4 over Ni/SiO_2 (65). Wang and Au (66) used CD_4 to resolve a kinetic isotope effect on Rh/SiO_2 catalyst and concluded that CH_4 dissociation is rate limiting and that CO_2 dissociation occurs prior to the surface reaction of CH_x fragments.

Reaction steps (b)–(d) represent the RWGS reaction and are at thermodynamic equilibrium ($\leftrightarrow$). Rostrup-Nielsen and Bak Hansen (14) have shown that turnover frequencies for the RWGS are typically much higher than for CH_4–CO_2 reforming and this reaction is essentially at thermodynamic equilibrium. Nondissociative adsorption of CO_2 during reaction occurs on the support, in the form of carbonates, as

proved by FTIR of CO_2 (Figs. 3 and 4). O'Connor (63) used *in situ* diffuse reflectance Fourier transform experiments to prove that very weakly adsorbed carbonate species are formed, once the lattice oxygen of zirconia has been replenished by CO_2. So, step (b) could be substituted for a more detailed set of reactions:

(b1) $2CO_2 + 2\mathbf{z} \rightarrow CO_3^{2-}\text{-}\mathbf{z} + \text{CO-}\mathbf{z}$,
(b2) $CO_3^{2-}\text{-}\mathbf{z} + 2\mathbf{z} \Leftrightarrow \text{CO-}\mathbf{z} + 2\ \text{O-}\mathbf{z}$,
(b3) $\text{CO-}\mathbf{z} \rightarrow \text{CO} + \mathbf{z}$.

The role of CO_2 is frequently assumed to be only a source of oxygen to the support. But CO_2 adsorbed species around the metal particle can react with CH_x fragments, as proposed in step (e), which was also proposed by Erdöhelyi *et al.* (67) and Raskó and Solymosi (68) in the metallic phase. This reaction is supposed to be irreversible because no methanation was observed over the platinum catalysts (Fig. 12), even at higher H_2 pressures (18). This is in contrast to that observed previously with either Ni/MgO or Ni/TiO_2 (23), but it is consistent with the observation of Vannice (69) that supported Ni is a better methanation catalyst than supported Pt.

The rate-determining steps in our model are the decomposition of CH_4 [step (a)] and the subsequent reaction of CH_x fragments with CO_2 adsorbed species [step (e)]. For catalysts that kinetically inhibit excessive carbon deposition, like zirconia-containing catalysts described here, the surface concentration of carbon at the metal surface (in the form of CH_x) is at steady state and remains constant (i.e., the rate of CH_x decomposition [step (a)] equals that for CH_x reaction with CO_2 adsorbed species [step (e)]). Assuming two independent balances of sites, the following reaction rate of methane was derived:

$$r_{CH_4} = \frac{k \cdot K_{CO_2} \cdot k_{CH_4} \cdot P_{CO_2} \cdot P_{CH_4}}{k \cdot K_{CO_2} \cdot P_{CO_2} + \left(1 + K_{CO_2} \cdot P_{CO_2}\right)\left(k_{CH_4} \cdot P_{CH_4} + k_{CH_4}^{-1} \cdot P_{H_2}^{4-x/2}\right)}.$$

This proposed kinetic model was fit to the data reported in Fig. 11, and the results for Pt10Zr catalyst are displayed in Fig. 13 at three different temperatures. The model fit very well the experimental data for zirconia-containing catalysts, but for PtAl the correlation was not good ($r = 0.972$), which was attributed to the deactivation of this catalyst during CH_4–CO_2 reforming, invalidating the hypothesis that the concentration of carbon remains constant.

The optimized kinetic parameters determined with this model for zirconia-containing catalysts are provided in Table 6. It is worth pointing out that the CO_2 adsorption constant, K_{CO_2}, is much higher for Pt10Zr than for the other catalysts. As the Pt10Zr catalyst exhibited a stable behavior during the reforming reaction between 823 and 1073 K, the stability (i.e., the coking resistivity) is likely related to the enhancement of the CO_2 adsorption on the support. Indeed, the higher stability of CO derived from CO_2 on Pt10Zr catalyst was shown by FTIR (Fig. 4). On

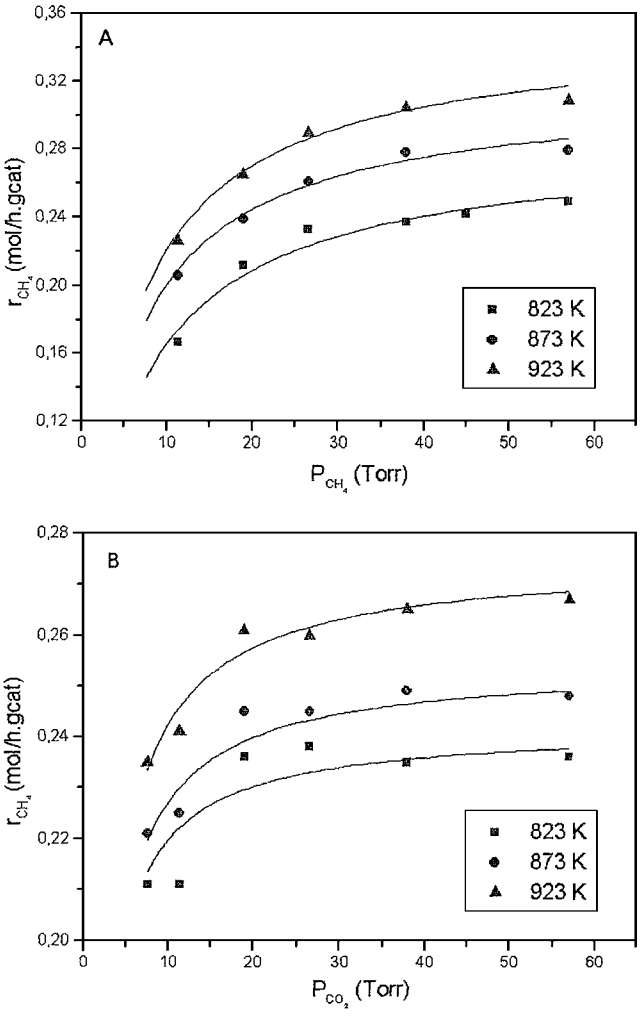

FIG. 13. Fit of the proposed kinetic model for CH_4–CO_2 reforming as a function of (A) methane partial pressure and (B) CO_2 partial pressure for the Pt10Zr catalyst.

the other hand, the reaction constant for step (e), k, is lower for the Pt10Zr catalyst, which displayed the best activity during catalytic tests. Thus, CH_4 decomposition is the rate-determining step of the reaction for a Pt10Zr catalyst,

TABLE 6

Optimized Kinetic Model Parameters

Parameters	PtZr (823 K)	Pt20Zr (823 K)	Pt10Zr 823 K	Pt10Zr 873 K	Pt10Zr 923 K
k_{CH_4}[a]	0.030	0.0406	0.0432	0.0595	0.0658
K_{CO_2}[b]	0.0148	0.0198	0.810	0.734	0.596
k[c]	1.138	0.996	0.296	0.330	0.369
Correlation[d]	0.983	0.993	0.999	0.999	0.999

[a] Units of mol/h · g cat · Torr.
[b] Units of $Torr^{-1}$.
[c] Units of mol/h · g cat.
[d] Obtained from the model fit to the dependence of CH_4 consumption rate on CO_2 partial pressure.

TABLE 7

Energetic Parameters from the Kinetic Model and the Literature (Kcal/mol)

Parameters	Pt10Zr[a]	Pt/TiO_2[b]	Ni/TiO_2[c]	ZrO_2[d]	Al_2O_3[d]
$E_{K CH_4}$	6.4	19	51	—	—
ΔH_{CO_2}	4.6	—	1	14–31	7.2
E_k	3.3	—	—	—	—

[a] From kinetic parameters in Table 6.
[b] Bradford and Vannice (18).
[c] Bradford and Vannice (23).
[d] Auroux and Gervasini (71).

while for the other catalysts CO_2 is involved in the slow step.

Plots of the model parameters listed in Table 6 for the Pt10Zr catalyst versus reciprocal temperature yielded the activation energy for step (a) in the forward direction, $E_{K_{CH_4}}$, the enthalpy of CO_2 adsorption, ΔH_{CO_2}, and the activation energy for step (e), E_k. These energy parameters are presented in Table 7, which also shows some values reported in the literature. The activation energy for CH_4 decomposition is lower than for Pt/TiO_2 (18) and for a elementary reaction on Pt(111) proposed by Shustorovich (70): $CH_4 + 2\mathbf{p} \rightarrow CH_3\text{-}\mathbf{p} + H\text{-}\mathbf{p}$, which reported an energy value of 12 Kcal/mol. The enthalpy of CO_2 adsorption is lower than the values for supports alone, presented by Auroux and Gervasini (71).

The lowering of the energy barrier for the Pt10Zr catalyst cannot be related to diffusional effects because rate data were taken under kinetic regime, far from thermodynamic equilibrium. So, it is proposed that a strong $Pt–Zr^{n+}$ interaction, which favors electron transfer from Pt to ZrO_2, lowers the energy barrier of the reaction.

CONCLUSIONS

These results showed that the support plays a decisive role in the activity and stability of the catalyst. PtAl deactivated quickly during the first 20 h of CH_4–CO_2 reforming at 1073 K, while zirconia-based catalysts (with ZrO_2 content $\geq$5%) presented improved stability over the course of 60 h. Sintering can be discarded and carbon deposition was very low on PtZr compared to PtAl catalyst, which was attributed to the $Pt–Zr^{n+}$ interfacial sites, which prevent coke formation and therefore enable high stability and activity of the zirconia-containing catalysts.

The dual site mechanism proposed for methane reforming with CO_2, considering the CH_4 decomposition and reaction of CH_x fragments with adsorbed CO_2 as slow kinetic steps, fits well with the experimental data for zirconia-containing catalysts. Calculated parameters of activation energy, enthalpy, and reaction or adsorption constants based on the rate-determining steps reinforce the hypothesis that there exists an interaction of Pt with Zr^{n+} centers during CH_4–CO_2 reforming. The calculated energy barrier is much lower than the apparent activation energy and supports the high and stable behavior of zirconia containing catalysts for CO_2 reforming of CH_4.

REFERENCES

1. Fischer, V. F., and Tropsch, H., *Brennst-Chem.* **3**(9), 39 (1928).
2. Lewis, W. K., Gilliland, E. R., and Reed, W. A., *Ind. Eng. Chem.* **41**, 1227 (1949).
3. Gadalla, A. M., and Bower, B., *Chem. Eng. Sci.* **43**, 3049 (1988).
4. Kurz, G., and Teuner, S., *Erdol. Kohle* **43**(5), 171 (1990).
5. Aparicio, L. M., *J. Catal.* **165**, 292 (1997).
6. Richardson, J. T., and Paripatyadar, S. A., *Appl. Catal.* **61**, 293 (1990).
7. Chubb, T. A., *Sol. Energy* **24**, 341 (1980).
8. Qin, D., and Lapszewicz, J., *Catal. Today* **21**, 551 (1994).
9. Udengaard, N. R., Hansen, J.-H. B., Hanson, D. C., and Stal, J. A., *Oil Gas J.* **90**(10), 62 (1992).
10. Teuner, S., *Hydrocarbon Process.* **64**, 106 (1985).
11. Teuner, S., *Hydrocarbon Process.* **66**, 52 (1987).
12. Erdöhelyi, A., Cserényi, J., and Solymosi, F., *J. Catal.* **141**, 287 (1993).
13. Zhang, Z. L., Tsipouriari, V. A., Efstathiou, A. M., and Verykios, X. E., *J. Catal.* **158**, 51 (1996).
14. Rostrup-Nielsen, J. R., and Bak Hansen, J. H., *J. Catal.* **144**, 38 (1993).
15. Bradford, M. C. J., and Vannice, M. A., *Catal. Rev.—Sci. Eng.* **41**(1), 1 (1999).
16. Bradford, M. C. J., and Vannice, M. A., *Catal. Today* **50**, 87 (1999).
17. Van Keulen, A. N. J., Hegarty, M. E. S., Ross, J. R. H., and van den Oosterkamp, P. F., *Stud. Surf. Sci. Catal.* **107**, 537 (1997).
18. Bradford, M. C. J., and Vannice, M. A., *J. Catal.* **173**, 157 (1998).
19. Bitter, J. H., Seshan, K., and Lercher, J. A., *J. Catal.* **171**, 279 (1997).
20. Bitter, J. H., Seshan, K., and Lercher, J. A., *J. Catal.* **176**, 93 (1998).
21. Stagg, S. M., Romeo, E., Padro, C., and Resasco, D. E., *J. Catal.* **178**, 137 (1998).
22. Stagg-Willims, S. M., Soares, R., Romeo, E., Alvarez, W. E., and Resasco, D. E., *Stud. Surf. Sci. Catal.* **130**, 3663 (2000).
23. Bradford, M. C. J., and Vannice, M. A., *Appl. Catal. A* **142**, 97 (1996).
24. Bradford, M. C. J., and Vannice, M. A., *Catal. Lett.* **48**, 31 (1997).
25. Noronha, F. B., Primet, M., Frety, R., and Schmal, M., *Appl. Catal.* **78**, 125 (1991).
26. Schmal, M., Souza, M. M. V. M., Aranda, D. A. G., and Perez, C. A. C., *Stud. Surf. Sci. Catal.* **132**, 695 (2001).
27. Damyanova, S., Grange, P., and Delmon, B., *J. Catal.* **168**, 421 (1997).
28. Yao, H. C., Sieg, M., and Plummer, H. K., Jr., *J. Catal.* **59**, 365 (1979).
29. Lieske, H., Lietz, G., Spindler, H., and Völter, J., *J. Catal.* **81**, 8 (1983).
30. Wagstaff, N., and Prins, R., *J. Catal.* **59**, 434 (1979).
31. Yao, H. C., and Yu Yao, Y. F., *J. Catal.* **86**, 254 (1984).
32. Yao, H. C., *Appl. Surf. Sci.* **19**, 398 (1984).
33. Baker, R. T. K., Prestridge, E. B., and Garten, R. L., *J. Catal.* **59**, 293 (1979).
34. Passos, F. B., Aranda, D. A. G., Soares, R. R., and Schmal, M., *Catal. Today* **43**, 3 (1998).
35. Bonneviot, L., and Haller, G. L., *J. Catal.* **130**, 359 (1991).
36. Vannice, M. A., and Sudhakar, C., *J. Phys. Chem.* **88**, 2429 (1984).
37. Hertl, W., *Langmuir* **5**, 96 (1989).
38. Guglielminotti, E., *Langmuir* **6**, 1455 (1990).
39. He, M.-Y., and Ekerdt, J. G., *J. Catal.* **87**, 238 (1984).
40. He, M.-Y., and Ekerdt, J. G., *J. Catal.* **87**, 381 (1984).
41. Mugniery, X., Chafik, T., Primet, M., and Bianchi, D., *Catal. Today* **52**, 15 (1999).
42. Morterra, C., Cerrato, G., and Pinna, F., *Spectrochim. Acta Part A* **55**, 9 (1999).

43. Brandt, R. K., Hughes, M. R., Bourget, L. P., Truszkowska, K., and Greenler, R. G., *Surf. Sci.* **286**, 15 (1993).
44. Bachiller-Baeza, B., Rodriguez-Ramos, I., and Guerrero-Ruiz, A., *Langmuir* **14**, 3556 (1998).
45. Swaan, H. M., Kroll, V. C. H., Martin, G. A., and Mirodatos, C., *Catal. Today* **21**, 571 (1994).
46. Bitter, J. H., Hally, W., Seshan, K., van Ommen, J. G., and Lercher, J. A., *Catal. Today* **29**, 349 (1996).
47. Bitter, J. H., Seshan, K., and Lercher, J. A., *J. Catal.* **183**, 336 (1999).
48. Seshan, K., ten Barge, H. W., Hally, W., van Keulen, A. N. J., and Ross, J. R. H., *Stud. Surf. Sci. Catal.* **81**, 285 (1994).
49. Roberts, S., and Gorte, R. J., *J. Phys. Chem* **95**, 5600 (1991).
50. Dilara, P. A., and Vohs, J. M., *J. Phys. Chem.* **99**, 17259 (1995).
51. Reitmeier, R. E., Atwood, K., Bennet, H. A., Jr., and Baugh, H. M., *Ind. Eng. Chem.* **40**, 620 (1948).
52. Efstathiou, A. M., Kladi, A., Tsipouriari, V. A., and Verykios, X. E., *J. Catal.* **158**, 64 (1996).
53. Van Santen, R. A., and Neurock, M., *Catal. Rev.—Sci. Eng.* **37**, 557 (1995).
54. Minot, C., van Hove, M. A., and Somorjai, G. A., *Surf. Sci.* **127**, 441 (1982).
55. Horiuchi, T., Sakuma, K., Fukui, T., Kubo, Y., Osaki, T., and Mori, T., *Appl. Catal. A* **144**, 111 (1996).
56. Zhang, Z. L., and Verykios, X. E., *Catal. Today* **21**, 589 (1994).
57. Narbeshuber, T. F., Brait, A., Seshan, K., and Lercher, J. A., *Appl. Catal.* **146**, 119 (1996).
58. Masai, M., Kado, H., Miyake, A., Nishiyama, S., and Tsuruya, S., *Stud. Surf. Sci. Catal.* **36**, 67 (1988).
59. Souza, M. M. V. M., Aranda, D. A. G., and Schmal, M., *in* "Simpósio Ibero-Americano de Catálise" (J. M. Órfão, J. L. Faria, and J. L. Figueiredo, Eds.), p. 141. Porto, Portugal, 2000.
60. Solymosi, F., Kutsan, G., and Erdöhelyi, A., *Catal. Lett.* **11**, 149 (1991).
61. Bodrov, I. M., and Apel'baum, L. O., *Kinet. Catal.* **8**, 326 (1967).
62. Mark, M. F., Mark, F., and Maier, W. F., *Chem. Eng. Technol.* **20**, 361 (1997).
63. O'Connor, A. M., Ph.D. dissertation, University of Limerick, Limerick, Ireland, 1998.
64. Van Keulen, A. N. J., Seshan, K., Hoebink, J. H. B., and Ross, J. R. H., *J. Catal.* **166**, 306 (1997).
65. Kroll, V. C. H., Swaan, H. M., Lacombe, S., and Mirodatos, C., *J. Catal.* **164**, 387 (1997).
66. Wang, W.-Y., and Au, C. T., *Appl. Catal. A* **155**, 239 (1997).
67. Erdöhelyi, A., Cserényi, J., Papp, E., and Solymosi, F., *Appl. Catal. A* **108**, 205 (1994).
68. Raskó, J., and Solymosi, F., *Catal. Lett.* **46**, 153 (1997).
69. Vannice, M. A., *J. Catal.* **74**, 199 (1982).
70. Shustorovich, E., *Adv. Catal.* **37**, 101 (1990).
71. Auroux, A., and Gervasini, A., *J. Phys. Chem.* **94**, 6371 (1990).